

Article

Improvement of Human Thermal Comfort by Optimizing the Airflow Induced by a Ceiling Fan

Hsin-Hung Lin 

Department of Creative Product Design, Asia University and Department of Medical Research, China Medical University Hospital, Taichung City 41354, Taiwan; hmlin@asia.edu.tw

Received: 25 March 2019; Accepted: 14 June 2019; Published: 18 June 2019



Abstract: The purpose of this study is to investigate the relationship between the greenhouse effect and the overuse of electricity and energy under a sustainable environment. The goal is to investigate the airflow that is induced by ceiling fans, by measuring human body temperature. In the simulation model, the thermal plume phenomenon is observed in the indoor environment. By changing the ceiling fan parameters, the influence of the airflow is investigated by practical measurement of human body temperature. The indoor convective heat transfer is enhanced by installing a ceiling fan, which affects the whole body thermal sensation (WBTS). Different scenarios are reviewed by adjusting the fan speed in the simulation model, so that the distribution of human body temperature can be determined. By modeling the blade plane of the ceiling fan, the airflow characteristics can be determined by making the simulation model rotate in order to assess the thermal comfort characteristics. As the ceiling fan generates circulation within the domain, the thermal comfort is significantly enhanced. By keeping a reasonable thermal comfort level, a higher room temperature or a higher heat load is allowed so that a sustainable environment can be maintained without affecting the indoor thermal comfort or the efficiency of energy usage.

Keywords: air distribution; CFD simulation; ceiling fan; interior temperature; thermal plume; convective boundary; buoyancy driven flows

1. Introduction

The topic of sustainable development deals with satisfying modern people's demands under the conditions of environmental protection, without affecting the needs of the next generations. The term "sustainable development" was originally proposed by the Brundtland Commission. They defined sustainable development as: "Sustainable development is development that meets the needs of the present without compromising the ability of future generations to meet their own needs." Therefore, it is important to reduce energy consumption and the greenhouse effect under this premise. Since one of the efficient ways of providing indoor cooling is by the use of ceiling fans, the goal of this study is to enhance thermal comfort without compromising energy consumption and the greenhouse effect. As ceiling fans provide thermal comfort with a lower level of power consumption, they are widely used inside all types of residential and commercial buildings [1,2]. Thermal comfort depends on a variety of factors, including the temperature, humidity, and air flow rate. The most beneficial effect of a ceiling fan is the convective heat transfer that is generated by the circulating fan, so that the indoor temperature distribution is more uniform [3,4]. A ceiling fan can increase the air speed, and therefore the correct use of a ceiling fan leads to better thermal comfort and a higher level of energy conservation. By generating airflow within a space, the convective heat transfer can be enhanced. Therefore, the air circulation that is generated within a room can improve the airflow distribution and enhance thermal comfort through the improved cooling of the human body. The cooling effect of a ceiling fan is affected by several fan parameters, including the rotating speed, diameter, blade count,

blade angle, and location [5–7]. By using a small circulating fan within a room, the room temperature can be increased to 28 °C when the air speed is in the range of 0.5 to 2 m/s, which can reduce the power consumption of air handling units. Based on the proposed method, the total reduction in power can be as high as 195.951 billion GWh/year [8]. An earlier study investigated the effect of using a ceiling fan of a 1200 mm diameter and a highest rotating speed of 240 RPM at a 3.0 m elevation within a room of 3.6 m × 3.6 m [9]. With a diameter of 1400 mm, they investigated the influence of different slant angles so that the blade tip speed was different [1]. They compared three commercially available ceiling fans to the fan specimen. Fan #1 had four blades; fan #2 had five blades and a larger motor; and fan #3 was roughly the same size as fan #2. In comparison, fan #4 was a prototype design that was aerodynamically improved by optimizing its blade design through numerical simulation. The airfoil was improved with a new design of a taper and twist in order to maximize the airflow. Fan #5 had the highest fan speed at the central portion of the impeller [10].

Simulations and experiments in earlier studies have indicated that the maximum simulated and experimental values of the time-averaged vertical velocity component are 0.226 m/s and 0.24 m/s, respectively [11]. Kurazumi studied the heat transfer coefficient for convection and radiation for human bodies. His emphasis was on the convective heat transfer area for human bodies. He used thermistors to measure the total heat flux and the radiation heat flux. The radiation heat transfer coefficient for a human body that sits on a chair with different postures was determined. He proposed empirical equations for the convective heat transfer coefficient, the driving temperature difference between the air and the body, and the average skin temperature under natural convection [12]. With four fans mounted on the four corners of a chair seat to generate upward airflow, Sun carried out a study of the increased effect of heat convection around a human body. His results indicated that the feeling of cooled air is enhanced at a higher room temperature of 26 °C, as the air passes the sensitive areas, including the lower legs, waist, legs, and arms. The recommended air velocity varies according to the room temperature: 0.48 m/s at 22 °C, 0.48 to 1.22 m/s at 24 °C, and 1.87 m/s at 26 °C. His results demonstrated that air movements around a human body do help reduce feelings of warmth, and therefore when the room temperature is at a higher level, the use of fans is recommended for air circulation [13]. For turbulence model simulation, Tham used the k - ϵ turbulence model (K-epsilon turbulence model) to model the airflow around a mannequin. The flow field inside a room with a mannequin and a desk, with a ventilation system, was analyzed by the computational fluid dynamics (CFD) commercial software, FLUENT 6.3. The assessment included the velocity field, the equivalent temperature of the mannequin, and the performance of the ventilation system at an ambient temperature of 26 °C [14]. The study by Liu indicated that the clothing thermal resistance is 0.5 CLO, and the metabolism rate is about 1 met when the relative humidity is 50% and the air velocity is less than 0.06 m/s. As the human body's thermal inertia changes according to its skin temperature and clothing, the experiment results indicated that the average skin temperature and feeling of warmth converge to stable values within 40 minutes. In a new thermal environment with an increasing temperature, the average/local skin temperature varies in a different way than the temperature in an environment with a decreasing ambient temperature, even when the radiation temperature is the same. The results of this study suggest that the human body temperature adapts to the surroundings in a different way depending on whether the ambient temperature is increasing or decreasing [15].

The goal of this study was to enhance the airflow that is generated by a ceiling fan, and to compare the results obtained by CFD simulation to the results obtained by real experiments. The study by Ho [3] simplified the geometry of a human body as a cylinder, without considering the details of a real human body. In a similar study by Makhoul [16], a heated cylinder was used to simulate the conditions of a human body in various types of environments. Therefore, the emphasis of this study was on the detailed geometry of a human body, so that the thermal comfort of the human body due to the indoor airflow conditions can be evaluated considering the complexity of human body geometry. By studying the thermal plume effect on a human body, the temperature distribution of the computer and the LCD monitor with the correct use of a ceiling fan was analyzed, in order to determine a higher level of

thermal comfort and a better effect of energy conservation. The improved ceiling fan designs, with better thermal comfort, could be a valuable contribution to maintaining a sustainable environment in tropical and subtropical regions.

2. Materials and Methods

2.1. Room Model and Configuration

Since the research target was the indoor airflow field in residential areas, the indoor computational domain used was $5.0\text{ m} \times 5.0\text{ m} \times 3.6\text{ m}$, as shown in Figure 1. A mannequin sits in the middle of the room with a height of 1.76 m and a total surface area of 2.1 m^2 . The dimensions were based on the data provided by Wang [17]. A ceiling fan was mounted on the central area of the ceiling. A computer and LCD (Liquid Crystal Display, LCD) monitor, with a total power consumption of 93 W, were placed on a desk in front of the mannequin [18].

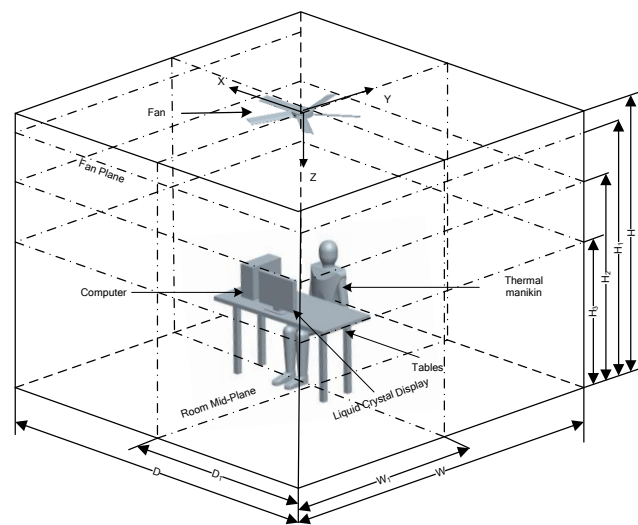


Figure 1. Configuration of the computational domain, including the ceiling fan, computer, LCD (Liquid Crystal Display) monitor, and the mannequin in the room.

2.2. Design Parameters of the Mannequin, Computer, and LCD Monitor

The simulation in this study was to determine the thermal comfort under a specific temperature for an indoor environment with the minimum energy cost. The mannequin height was about 1.76 m. The surface temperature of this mannequin was determined by numerical methods. There were a total of 19 monitoring points on the mannequin, as shown in Figure 2a. These monitoring points included the head, chest, back, abdomen, hip, upper arm, lower arm, hand, thigh, lower leg, and feet. There were a total of nine monitoring points on the LCD monitor, including its top, front, and rear panels, as shown in Figure 2b,c. There were five monitoring points on the computer, as shown in Figure 2d. Therefore, the total number of monitoring points in this system was 34. The variation in the temperature of each monitoring point was recorded in order to understand the influence of the airflow generated by the ceiling fan on the human body's surface temperature [2].

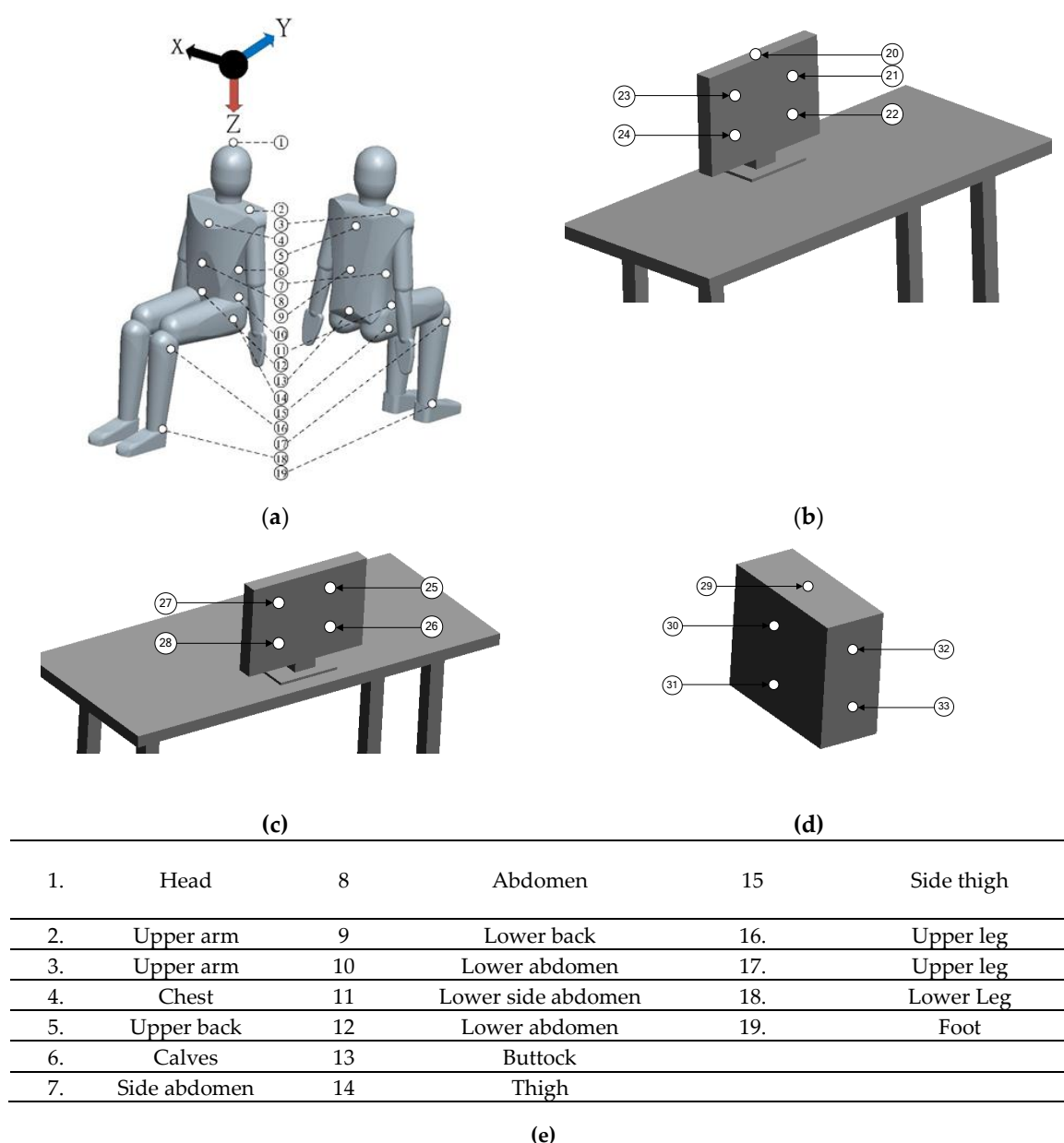


Figure 2. Monitoring points on the human body, computer, and LCD monitor: (a) Monitoring points on the human body; (b) monitoring points on the front panel of the LCD monitor; (c) monitoring points on the rear panel of the LCD monitor; (d) monitoring points on the computer; (e) descriptions of 19 measurement points.

2.3. Methods

2.3.1. Numerical Analysis

The airflow and temperature distribution of a computational domain can be determined by numerical simulation. Examples of indoor airflow patterns and temperatures from earlier studies are based on the standard $k-\epsilon$ model, and the configuration of CFD (Contract For Difference) boundary conditions [19,20]. Ankur et al. [21] also used the standard $k-\epsilon$ model to calculate the indoor thermal environment of an office with a ceiling cooling system. The numerical results of the indoor airflow and temperature distribution were quite accurate [7].

In three-dimensional Cartesian coordinates, the governing equations are as follows (FLUENT User's Guide).

(1) Continuity equation:

$$\frac{\partial u}{\partial x} + \frac{\partial v}{\partial y} + \frac{\partial w}{\partial z} = 0 \quad (1)$$

(2) Momentum equations: X direction:

$$\frac{\partial u}{\partial t} + \frac{\partial(u^2)}{\partial x} + \frac{\partial(uv)}{\partial y} + \frac{\partial(uw)}{\partial z} = -\frac{1}{\rho} \frac{\partial P}{\partial x} + \nu \left[\frac{\partial^2 u}{\partial x^2} + \frac{\partial^2 u}{\partial y^2} + \frac{\partial^2 u}{\partial z^2} \right] \quad (2)$$

Y direction:

$$\frac{\partial v}{\partial t} + \frac{\partial(uv)}{\partial x} + \frac{\partial(v^2)}{\partial y} + \frac{\partial(vw)}{\partial z} = -\frac{1}{\rho} \frac{\partial P}{\partial y} + \nu \left[\frac{\partial^2 v}{\partial x^2} + \frac{\partial^2 v}{\partial y^2} + \frac{\partial^2 v}{\partial z^2} \right] \quad (3)$$

Z direction:

$$\frac{\partial w}{\partial t} + \frac{\partial(uw)}{\partial x} + \frac{\partial(vw)}{\partial y} + \frac{\partial(w^2)}{\partial z} = -\frac{1}{\rho} \frac{\partial P}{\partial z} + \nu \left[\frac{\partial^2 w}{\partial x^2} + \frac{\partial^2 w}{\partial y^2} + \frac{\partial^2 w}{\partial z^2} \right] \quad (4)$$

(3) Energy equation:

$$\frac{\partial T}{\partial t} + \frac{\partial(uT)}{\partial x} + \frac{\partial(vT)}{\partial y} + \frac{\partial(wT)}{\partial z} = \alpha \left(\frac{\partial^2 T}{\partial x^2} + \frac{\partial^2 T}{\partial y^2} + \frac{\partial^2 T}{\partial z^2} \right) + \frac{q}{\rho C_p} \quad (5)$$

(4) Governing equations can be represented by the general equations as follows:

$$\frac{\partial(\rho\phi)}{\partial t} + \frac{\partial(\rho\phi u)}{\partial x} + \frac{\partial(\rho\phi v)}{\partial y} + \frac{\partial(\rho\phi w)}{\partial z} = \frac{\partial}{\partial x} \left(\Gamma \frac{\partial\phi}{\partial x} \right) + \frac{\partial}{\partial y} \left(\Gamma \frac{\partial\phi}{\partial y} \right) + \frac{\partial}{\partial z} \left(\Gamma \frac{\partial\phi}{\partial z} \right) + S \quad (6)$$

where $\frac{\partial(\rho\phi u)}{\partial x} + \frac{\partial(\rho\phi v)}{\partial y} + \frac{\partial(\rho\phi w)}{\partial z}$ is the convective term, $\frac{\partial}{\partial x} \left(\Gamma \frac{\partial\phi}{\partial x} \right) + \frac{\partial}{\partial y} \left(\Gamma \frac{\partial\phi}{\partial y} \right) + \frac{\partial}{\partial z} \left(\Gamma \frac{\partial\phi}{\partial z} \right)$ is the diffusive term, S is the source term, and $\frac{\partial(\rho\phi)}{\partial t}$ is the unsteady term and is not considered when the system is in the steady state. The symbol represents physical variables, such as u , v , w , k , ε , and T (Table 1). The velocity components in the x , y , and z directions are, respectively, u , v , and w . Γ is the corresponding diffusivity of each physical variable. Since we are looking for a steady-state solution, the variables are independent of time. Therefore, the partial derivatives of u , v , w , and T with respect to t are equal to zero.

Table 1. Symbols of independent variables.

Continuity	1
X-momentum	u
Y-momentum	v
Z-momentum	w

2.3.2. Standard k - ε Turbulence Model

Due to its wide range of applications and reasonable accuracy, the standard k - ε model has become one of the dominant tools for the calculation of the turbulent flow field. The standard k - ε model is a semi-empirical turbulence model, which can be used to derive the transport equations for the turbulent kinetic energy (k) and the rate of dissipation (ε) based on fundamental physical control equations. The equations are as follows.

Turbulent kinetic energy (k):

$$\frac{\partial}{\partial t}(\rho k) + \frac{\partial}{\partial x_i}(\rho k u_i) = \frac{\partial}{\partial x_j} \left[\left(\mu + \frac{\mu_t}{\sigma_k} \right) \frac{\partial k}{\partial x_j} \right] + G_k + G_b - \rho \varepsilon - Y_M. \quad (7)$$

Rate of dissipation (ε):

$$\frac{\partial}{\partial t}(\rho \varepsilon) + \frac{\partial}{\partial x_i}(\rho \varepsilon u_i) = \frac{\partial}{\partial x_j} \left[\left(\mu + \frac{\mu_t}{\sigma_\varepsilon} \right) \frac{\partial \varepsilon}{\partial x_j} \right] + C_{1s} \frac{\varepsilon}{k} (G_k + C_{3\varepsilon} G_b) - C_{2g\rho} \frac{\varepsilon^2}{k}. \quad (8)$$

Turbulent viscosity (μ_t):

$$\mu_t = \rho C_\mu \frac{k^2}{\varepsilon}, \quad (9)$$

where G_k indicates the turbulent kinetic energy due to the laminar velocity gradient, G_b represents the turbulent kinetic energy due to buoyancy, Y_M deals with the fluctuations due to the excessive diffusion within compressible turbulent flows, σ_k and σ_ε are the turbulent Prandtl numbers of turbulent kinetic energy and turbulent dissipation, and $C_{1\varepsilon}$, $C_{2\varepsilon}$, and $C_{3\varepsilon}$ are empirical constants. Their recommended values are shown in Table 2.

Table 2. Empirical constants of the standard k - ε turbulence model (K-epsilon turbulence model).

$C_{1\varepsilon}$	$C_{2\varepsilon}$	C_u	C_k	$C_{3\varepsilon}$
1.44	1.92	0.09	1.0	1.3

2.3.3. Boundary Conditions

The boundary conditions for the computational domain in this study are shown in Table 3. The indoor ambient air temperature was set at 25 °C. A ceiling fan was mounted on the central portion of the ceiling and directly above the mannequin's head, the computer, and the LCD monitor. The heat dissipation of the mannequin was set at 70 W. The heat dissipation of the computer in front of the mannequin to the right hand side was set at 93 W. The LCD monitor in front of the mannequin was set at 95 W [22]. Moreover, the ceiling fan's rotating boundary condition was set at 240 RPM/200 RPM/160 RPM. In the numerical model, the flow passage between the fan blades rotates around the fan's origin of coordinates. The fluid must meet the boundary condition of impermeable walls.

Table 3. Boundary conditions and parameters of the numerical simulation.

Configuration of environment	Indoor conditions	Air temperature: 25 °C		
		Boundary conditions	No-slip condition	
	Pressure	Static pressure is 0		
Walls and furniture	Furniture, walls	No-slip condition Material: solid smooth surface Heat dissipation: none		
Heat source	Mannequin	Heat dissipation: 70 W [12,22]		
	Computer	Heat dissipation: 93 W [22]		
	LCD monitor	Heat dissipation: 95 W [22]		
Ceiling fan	Rotating boundary	The flow passages between fan blades are rotating around the fan's origin of coordinates. The rotating speed is set as follows.		
		Case 1	Case 2	Case 3
		240 RPM	200 RPM	160 RPM
	Fixed boundary	Fluid needs to satisfy both the impermeable condition and the no-slip condition at walls.		

2.3.4. Numerical Simulation and Analysis

The numerical simulation in this study was to determine the interactions between the ceiling fan's rotating speed, human body temperature, the computer temperature, and the LCD monitor temperature. A total of 12 males were invited to participate in the body comfort questionnaire survey. These participants were aged 25 to 35 years old with their heights in the range of 170 to 179 cm and their weights in the range of 75 to 80 kg. Therefore, it was important to create a correct physical model for the system in order to predict the influence of the turbulence model and the boundary conditions on the thermal environment [18]. Variations in the air flow field, thermal field, and the human body's thermal plume were determined by the numerical simulation. In order to create a correct CFD model, several methods have been proposed for understanding the airflow characteristics due to a ceiling fan [23]. Since this study concerned the diffusion of the airflow to the human body, computer, and LCD monitor, the kinetic energy equation was used. Moreover, it can be observed from the velocity profile of the cross section along the ceiling fan that the turbulence intensity and the temperature variation within the stagnated indoor air are very important characteristics. For the calculation of this domain, the boundary condition and the quality of meshes are equally important. Therefore, for the location regions around the mannequin, the computer, and the LCD monitor, the mesh should be further refined. As a result, the mesh count for the ceiling fan was 137,412, that for the computer and the LCD monitor was 1,631,057, and that for the mannequin was 1,631,057. A cross-sectional view of the mesh structure is shown in Figure 3.

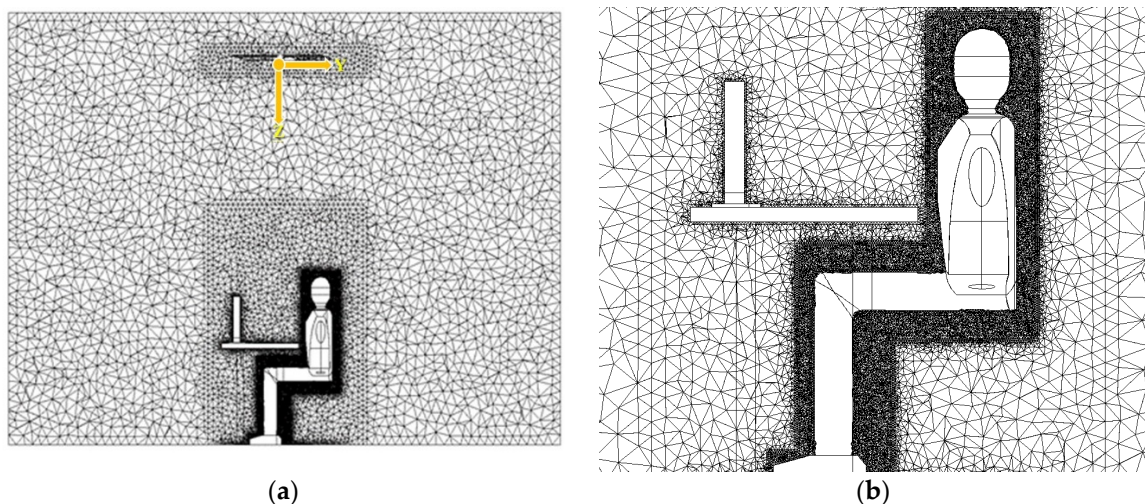


Figure 3. Mesh structure: (a) Cross-sectional view of the room; (b) cross-sectional view of the computer, LCD monitor, and the mannequin.

2.3.5. Apparatus and Equipment for Experiments

The experiments were carried out in southern Taiwan, and the dimensions of the room were 5.0 m × 5.0 m × 3.6 m. A desk was located in the central area of the room, along with a computer, an LCD monitor, and a ceiling fan with five blades. The ceiling fan was equipped with a DC controller (domain controller, DC) for controlling its rotating speed. A male participant carried out the experiment, and his clothes had a clothing thermal resistance of 0.55 to 0.6 CLO [23,24]. During the experiments, the indoor air temperature was within the range of 25 to 26 °C, which was measured by a TECPEL DTM-323 temperature and humidity sensor. The measurement tolerance of this sensor is ±0.5 °C and ± 3% RH.

A total of 19 thermistors were attached to the skin of the participant's body, including top head, chest, left arm, right arm, top back, abdomen front, abdomen left, abdomen right, back middle, lower abdomen front, lower abdomen left, lower abdomen right, thigh right, thigh left, lower leg right, lower leg left, left foot, right foot, and lower back. The temperature and air velocity were recorded every

10 s by the Agilent 34970A, which is a 20-channel multiplexer module, and the TESTO 405-V1 mini hotwire anemometer. The temperature measurement tolerance was $\pm 0.1\text{ }^\circ\text{C}$ and $\pm 0.1\text{ m/s}$. The average radiation temperature was not measured in this study, and we assumed it to be the same as the indoor air temperature. The experiments were carried out by setting the ambient temperature at $26\text{ }^\circ\text{C}$ and the relative humidity at 55%. The relative location of the ceiling fan, mannequin, computer, and LCD monitor are shown in Figure 4.

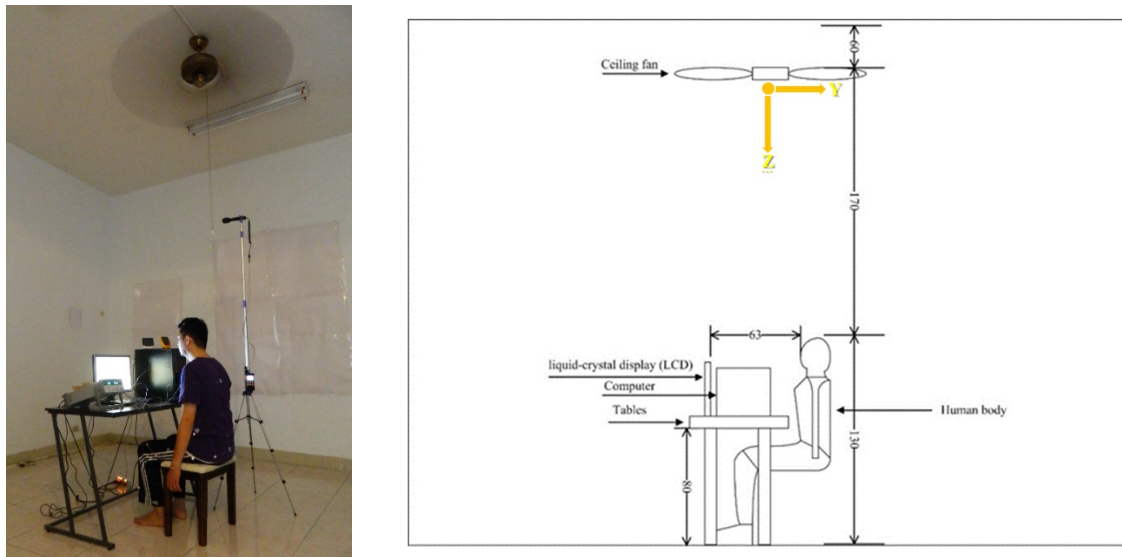
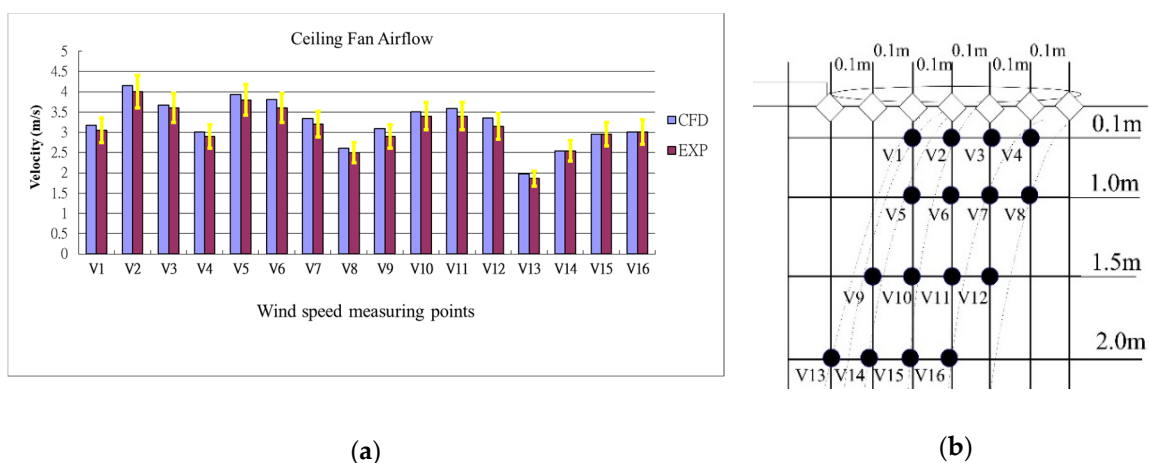


Figure 4. Location of the ceiling fan, human body, computer, and LCD monitor.

Before the experiments started, the hotwire anemometer was calibrated by measuring the air velocity within the target range of the rotating speed for the ceiling fan. The air velocity was recorded at a total of 28 different points directly under the coverage area of the ceiling fan. With a nozzle at the outlet of a horizontal pole, the anemometer was triggered to measure the air velocity and convective flow intensity. The simulation results were compared to the experimental results in Figure 5, in which blue lines indicate the CFD simulation results and red lines indicate the experimental results. The yellow lines indicate the range of 10% error [22]. There were 16 monitoring points for the anemometer measurement and these points are marked as V1 to V16. In general, the results in Figure 5 indicate an error of 3.6% between the simulated and the measured results.



(a)

(b)

Figure 5. Comparison of (a) measured results; (b) simulated results.

In addition to the measurement and verification of the airflow velocity, the skin temperature of the human body was also recorded at 19 different locations. To ensure correct measurement of the skin temperature, the participant was asked to rest for 30 minutes after each round of experiments, so that his/her body temperature could return to its original status before each round of testing. The body temperature during the testing of these three cases was then recorded, as shown in Figure 6. For all of these cases, the ambient temperature was controlled at 26 °C. These body temperature values were compared to the results that were obtained by CFD simulation, and the average resulting difference between the measured and the simulated values was 3.7%, which does not exceed the uncertainty of the apparatus that was used for measurement.

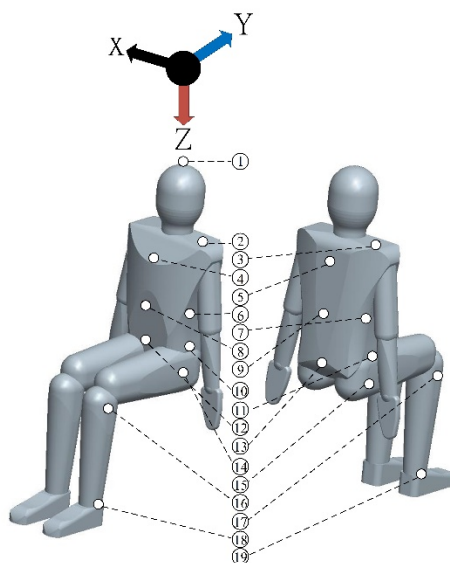
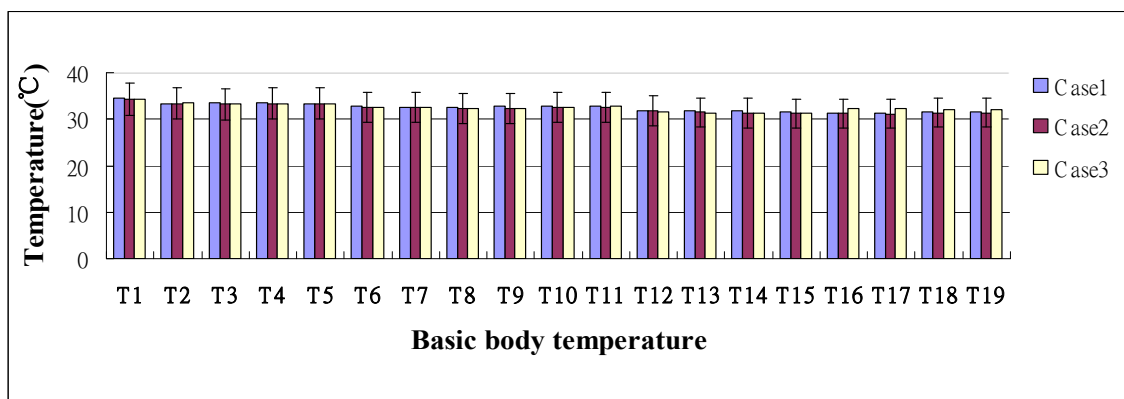


Figure 6. Measured body temperature at 19 monitoring points.

In addition, based on the results obtained by the ceiling fan air flow and momentum equation, the mesh around the human body needs to be refined for better results. Therefore, the mesh was restructured for the CFD model, and the resulting values that were obtained by the simulation were compared to the measured results.

3. Results

3.1. Influence of the Ceiling Fan on the Indoor Airflow

3.1.1. Three-Dimensional Velocity Distribution of the Airflow Directly under the Ceiling Fan

The velocity distribution of the air flow under the ceiling fan at the elevations of $Z = 0.1$ m, $Z = 1.0$ m, and $Z = 1.5$ m is shown in Figure 7. The airflow patterns at different elevations can be

visualized from these figures, as the cone shape clearly indicates the higher air velocity under the ceiling fan. Moreover, five protrusions with a needle shape are observed in Figure 7a; these are the locations of the blade tips with the highest air velocity. In Figure 7b, due to the reacting flow from the floor, the needle-shape protrusions disappear, while the air velocity is also reduced. The reduction in the back pressure due to the floor leads to the slightly increased air velocity shown in Figure 7c. Due to the air viscosity and the molecular attraction, the momentum is transformed downward from the rotating ceiling fan to the region that is near the floor.

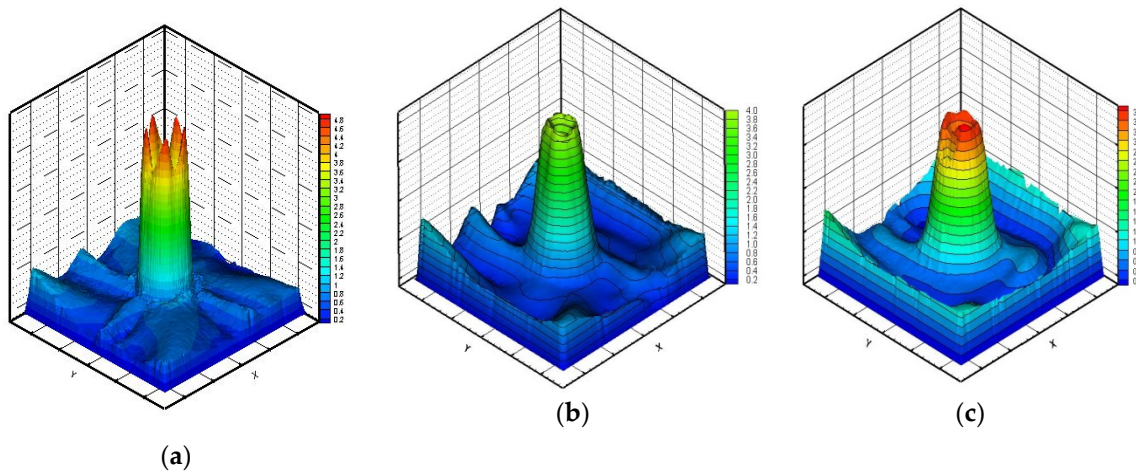


Figure 7. Qualitative velocity distribution at different elevations: (a) $Z = 0.1$ m below the ceiling fan; (b) $Z = 1.0$ m below the ceiling fan; (c) $Z = 1.5$ m below the ceiling fan.

3.1.2. Contour of Velocity Magnitude at Cross-Sectional Planes

To further investigate the airflow characteristics, the contour of the velocity magnitude at cross-sectional planes below the ceiling fan is shown in Figure 8. The contours at both the X and the Y planes clearly indicate a pattern of outward air diffusion. Moreover, due to the combined effect of the no-slip condition on the wall and the backward pressure from the floor, the downward air velocity is gradually reduced. The gradual change in air velocity is one of the important factors of this flow field. The airflow is also affected by the existence of the computer and the desk. The resulting air velocity to the region near the floor can be observed in Figure 8a. From the Y-plane in Figure 8b, the airflow splits due to the existence of the desk and the human body, moves both sides toward the floor, and finally makes a strong recirculation.

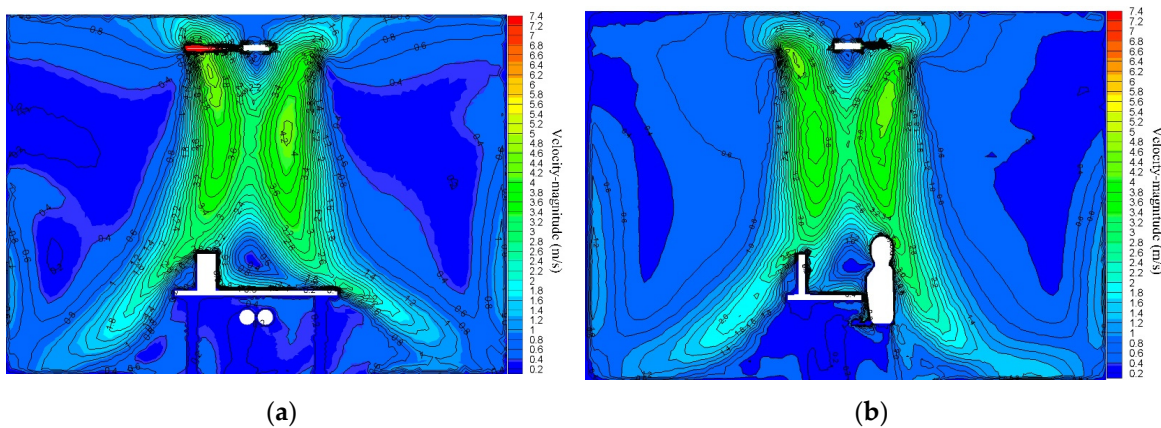


Figure 8. Contour of the velocity magnitude in m/s at different cross-sectional planes: (a) X-plane; (b) Y-plane.

The velocity profile in Figure 9 also indicates that the downward airflow is affected by the existence of the desk and the human body. The change in the flow field is a desired phenomenon for the cooling effect by the ceiling fan, since human body heat can be effectively moved away by the resulting airflow.

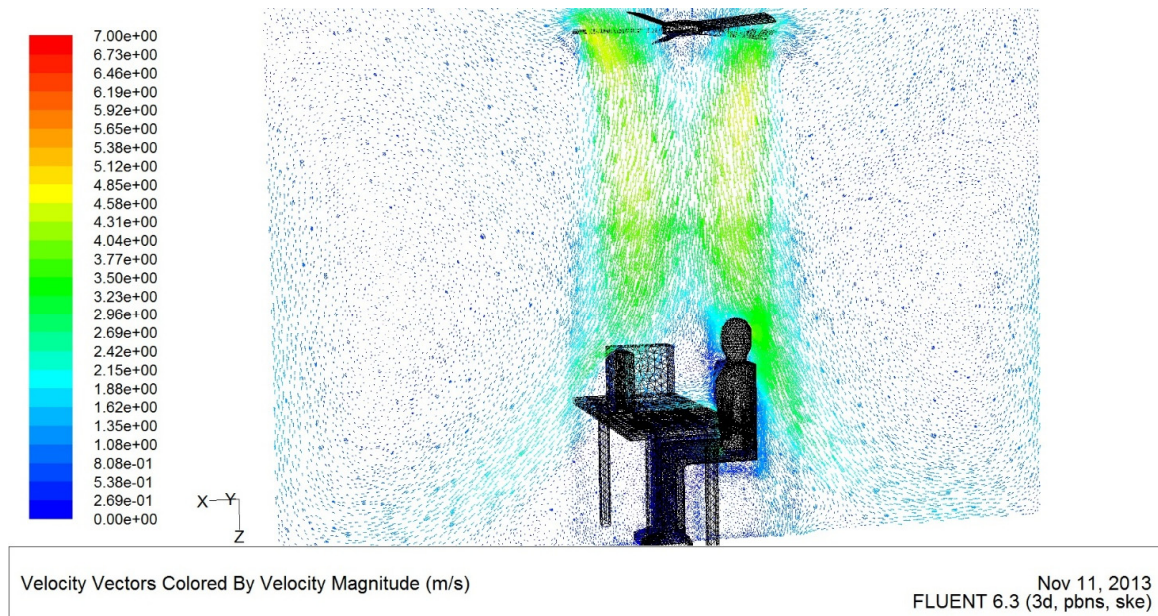


Figure 9. Velocity profile of the radial velocity distribution along the central plane.

3.1.3. Comparison of the Simulated and the Measured Values of the Velocity Components

Figure 10 shows the airflow characteristic curves of the simulated and measured results for the ceiling fan airflow. The velocity magnitude, f , is determined by Equation (10) as follows, where u , v , and w are the velocity components in the x , y , and z directions, respectively. As shown in Figure 10, the velocity magnitudes at $Z = 0.1, 1, 1.5$, and 2.0 m indicate that the maximum magnitude is more than 4.0 m/s between the radial distance of 0 and 0.7 m. Basically, the velocity magnitude at any location beyond 0.7 m can be neglected:

$$f = \sqrt{u^2 + v^2 + w^2}. \tag{10}$$

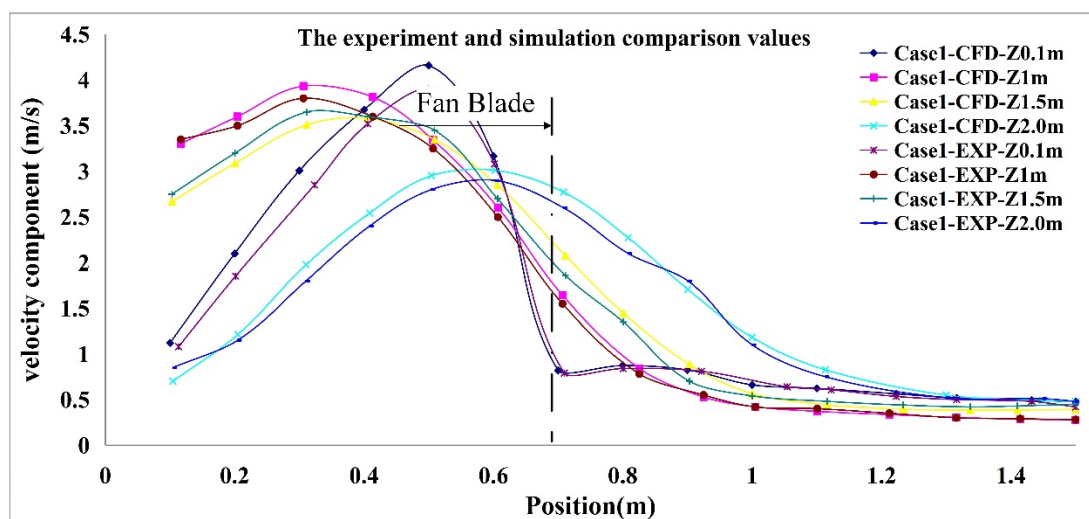


Figure 10. Velocity components at different locations for case 1.

3.2. Indoor Temperature Distribution

3.2.1. Distribution of Lines of Equal Temperature

Figure 11 shows the temperature distribution of the solution domain by CFD simulation. Since the ceiling fan generates the airflow that allows the mixture of warm and cool air, the air temperature decreases along the walls and the floor at a relatively lower speed. The heat transfer is mainly through thermal diffusion. The lines of equal temperature in Figure 11a indicate the temperature difference of the air flowing through the LCD monitor, desk, and the human body along the X-plane. On the Y-plane, as shown in Figure 11b, the temperature gradient of the air that flows through the LCD monitor and the desk can also be observed.

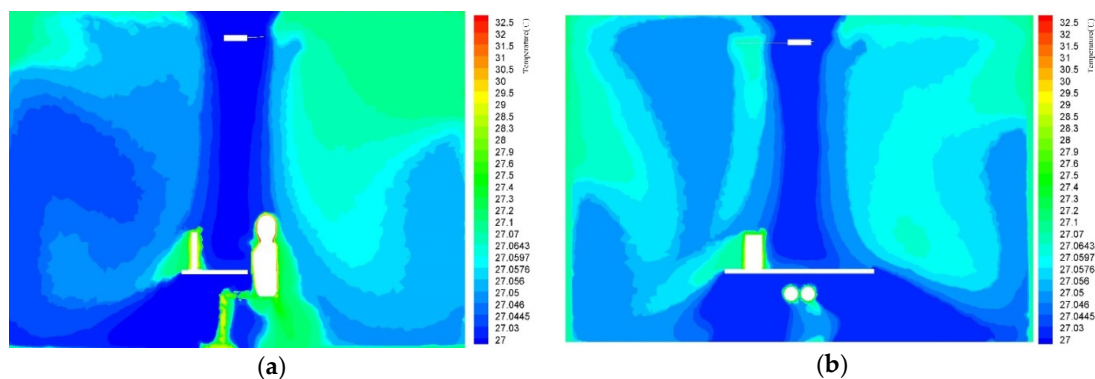


Figure 11. Distribution of lines of equal temperature: (a) X-plane; (b) Y-plane.

The overall thermal comfort can be determined from the combined effect of the air velocity and the reduced air temperature. This effect is further verified by the measurement of the whole body thermal sensation (WBTS) on various locations of the human body.

3.2.2. Air Velocity on the Surface of the Human Body

To verify the optimal air velocity suggested by the CFD simulation results, we carried out experiments on the optimal thermal plume in the indoor domain. The result of case 1 indicates that when the airflow passes the human body's head, it affects the thermal conditions around this domain. When the ambient temperature is 26.5 °C, the airflow reaches the highest velocity of 1.92 m/s. However, the thermal plume does not occur when the air velocity is greater than 0.2 m/s [25]. Therefore, the higher air impedance leads to a better effect that can be generated by the thermal plume, as shown in Figure 12. The results of the experiment also indicate that it could be difficult to keep the head temperature and the leg temperature in the same range. As a result, the ambient temperature difference should be kept at the minimum level so that the change in the human body temperature can be minimized.

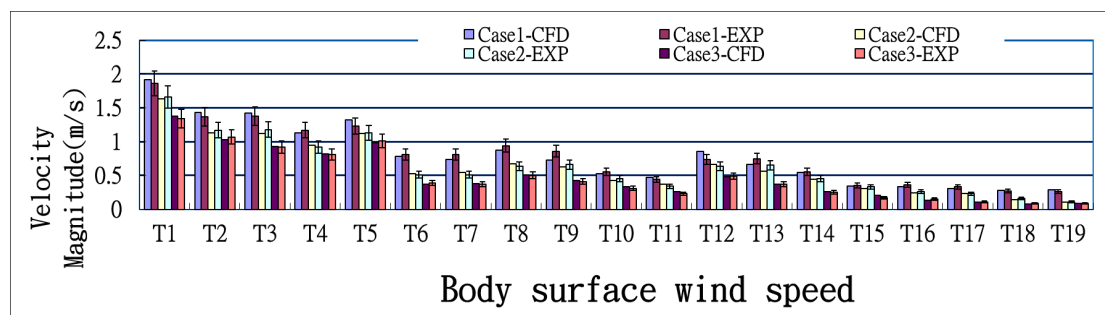


Figure 12. Comparison of the human body's surface air velocity from the CFD simulation result to those from the experiments.

To ensure that the remaining heat within the environment did not affect the next round of experiments, the computer and the LCD monitor were switched off for 30 minutes before another round of experiments started. The results in Figure 13 indicate that the human body temperature varies depending on the air velocity, as case 3 has the lowest rotating speed and case 2 has a higher speed. When the ceiling fan airflow system is operating at a lower rotating speed, case 3 has a similar temperature distribution to case 2. This phenomenon is especially apparent at the lower half of the human body. By studying the airflow field of these three cases, the goal of this study was to determine the thermal comfort and the feeling of warmth due to the airflow generated by the ceiling fan. With optimal conditions of ventilation, the thermal plume on the human body can be reduced, since the airflow passes the human body and moves along the floor in all directions. This phenomenon realizes better conditions of air mixture.

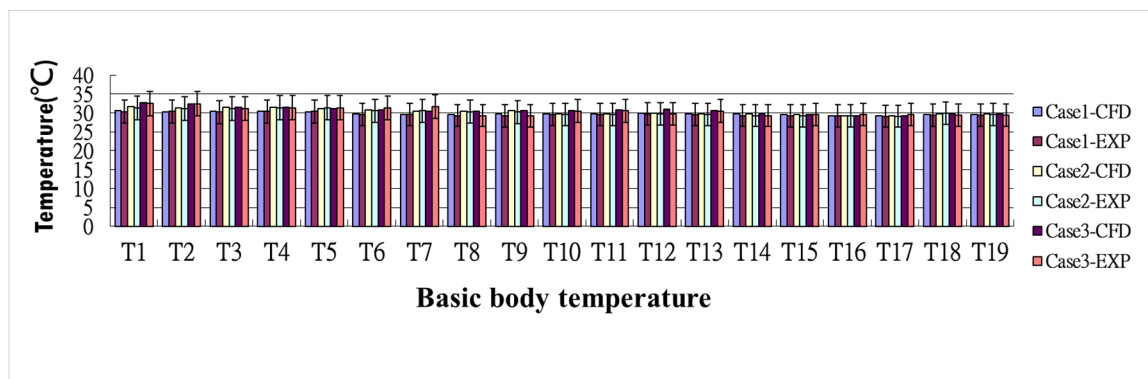


Figure 13. Comparison of the human body's surface temperature from the CFD simulation result to those from experiments.

3.2.3. Measurement of Temperature around the Human Body

One of the important factors of this study was the temperature around the human body. As shown in Figure 14, the temperature readings at the skin surface, 1 cm from the skin, and 3 cm from the skin were recorded for 19 monitoring points. The results indicated that case 1's temperature distribution is more uniform on average, since it has a higher air velocity. On the other hand, case 3's temperature distribution is relatively non-uniform, with a larger variation and asymmetric temperature distribution. Since the thermal dissipation effect at the human body's head is much higher than at the other positions, the thermal plume disappears at an earlier stage due to the mixture of the air around this domain. The radar chart of case 1 in Figure 14 indicates a uniform distribution for the monitoring locations with higher air velocity.

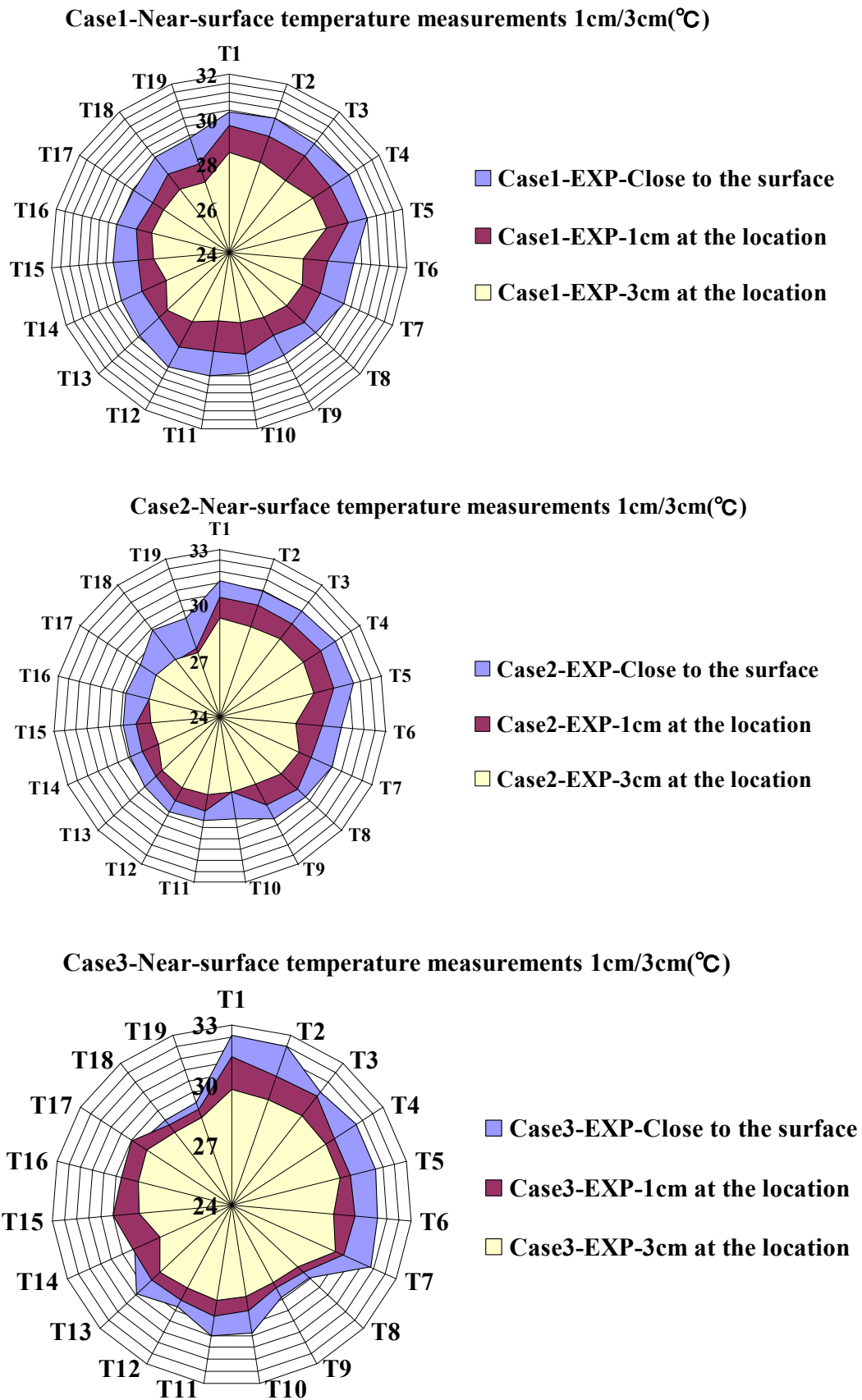


Figure 14. Temperature readings of 19 monitoring points on the skin surface, 1 cm from the skin, and 3 cm from the skin for case 1, 2, and 3.

3.2.4. Effect of Air Velocity on the Temperature at Monitoring Points

Since the purpose of this study was to investigate the effect of the ceiling fan airflow on the temperature of different portions of the human body, the participants were asked to wear clothes with a clothing thermal resistance of 0.55 to 0.6 CLO. The experiment was carried out under an ambient temperature of 26 °C. By adjusting the ceiling fan's rotating speed, the participants were asked to record their temperature experience on a 7-point scale, which included "uncomfortably cold," "cold," "cool," "comfortable (neither cold nor warm)," "slightly warm," "warm," and "uncomfortably warm." Most of the participants felt "cold" during the test of case 1, while they felt "comfortable (neither cold nor warm)" during the test of case 3. Therefore, the desired condition of thermal comfort can be achieved by adjusting the ceiling fan's rotating speed to a relatively lower RPM. This result is similar to those obtained by earlier studies [11]. When the ceiling fan was turned on, the participants felt cold at the top portion of their body, while they felt slightly warm at the lower body portions. By setting the fan speed at the optimal RPM, thermal comfort can be achieved in a more effective way without consuming much energy.

For the three cases under investigation, case 3 delivered the optimal level of thermal comfort. By comparing the temperature at the monitoring points to the air velocity for case 3, the distribution of the human body's temperature can be determined. The measurement results also indicate that a ceiling fan can effectively reduce the indoor temperature using an optimal mixture of cool and warm air. As shown in Table 4, the simulation results match well to the real measurement results obtained in the experiment for different portions of the human body. Therefore, the ceiling fan does change the thermal condition of the target domain by generating more convective heat transfer effects to reduce the indoor temperature.

Table 4. Comparison of terminal temperature and terminal velocity for the human body, the computer, and the LCD monitor.

(a) Body	Temperature measuring points																			
	1	2	3	4	5	6	7	8	9	10	11	12	13	14	15	16	17	18	19	
Terminal temp (°C)	EXP	32.5	32.4	31.2	31.4	31.4	31.3	31.6	29.3	29.2	30.5	30.6	29.8	30.5	29.3	29.6	29.6	29.4	29.4	
	CFD	32.7	32.3	31.5	31.5	31.2	30.8	30.5	30.5	30.7	30.7	30.8	30.9	30.7	29.8	29.5	29.3	29.3	29.8	29.8
Terminal velocity (m/s)	EXP	1.34	1.07	0.92	0.81	1.01	0.39	0.37	0.50	0.41	0.31	0.23	0.49	0.37	0.25	0.17	0.15	0.11	0.09	0.09
	CFD	1.38	1.03	0.93	0.82	0.98	0.37	0.38	0.51	0.43	0.33	0.26	0.48	0.37	0.26	0.21	0.13	0.11	0.08	0.09
(b) Computer	Temperature measuring points																			
	20	21	22	23																
Terminal temp (°C)	EXP	32.42	32.54	32.75	32.6															
	CFD	33.21	33.23	33.67	32.87															
Terminal velocity (m/s)	EXP	1.18	0.68	0.42	0.45															
	CFD	1.25	0.62	0.36	0.42															
(c) LCD monitor	Temperature measuring points																			
	24	25	26	27																
Terminal temp (°C)	EXP	31.6	31.4	31.8	32.3															
	CFD	32.4	32.6	33.7	33.7															
Terminal velocity (m/s)	EXP	1.25	0.51	0.34	0.37															
	CFD	1.24	0.54	0.37	0.41															

For a typical office with an area of 90 m³, the minimum power consumption of a central air conditioner is 1000 W [26,27]. Therefore, if the central air conditioner is turned on 8 h a day, 20 days a month, and assuming it works six months per year, the annual power consumption is 1920 kWh per year for this office of 90 m³. In comparison, if the central air conditioner is replaced with a ceiling fan which operates at the highest rotating speed, its power consumption is 60 W and the annual power consumption is only 7.2 kWh per year. Therefore, the energy saving can be up to 1804.8 kWh per year for this office of 90 m³ [28,29].

4. Conclusions

One of the important topics for the design of a sustainable and healthy environment is the supply of air that provides thermal comfort for human bodies within an office. In addition to improving indoor air recirculation, a ceiling fan can also provide thermal comfort without the need for an air conditioner. Therefore, a ceiling fan can create a sustainable environment at the lowest energy cost. For air recirculation within a building, a ceiling fan can be mounted directly above a computer desk in order to provide the required convective heat transfer. The findings of this study were as follows.

1. For a sustainable environment, a ceiling fan is one of the most effective solutions to resolve the problems of the greenhouse effect and the excessive use of electric power.
2. For an indoor environment with a ceiling fan, the simulation results indicated that the maximum allowable indoor temperature is 32.5 °C and the minimum allowable temperature is 29.3 °C with the thermal effect, due to the air recirculation that is generated by the ceiling fan.
3. In this study, it was found that the air velocity is reduced as the air approaches the floor. Moreover, the airflow is also affected by the arrangement of the human body and the locations of furniture, which affect the indoor airflow.
4. The results of this study indicated that the thermal plume that is generated by the human body is affected by a downward airflow at a velocity of 0.3 m/s, and the heat that is generated by the human body will diffuse in all directions.
5. The potential power saving is 1804.8 kWh per year for an office of 90 m³ if a ceiling fan is used instead of an air conditioner. This value is similar to the findings in earlier studies.
6. The CFD simulation results and the measurements indicated that optimal thermal comfort can be achieved for the human body if the air velocity is 1.34 m/s when the airflow reaches the top of the head.

When using a ceiling fan to create a sustainable environment, the air convective heat transfer allows the ceiling fan to create a uniform temperature distribution within a room. However, the recirculation also keeps a small portion of heat within this room, so that the overall temperature is slightly increased. Further studies are advised to figure out a way of increasing the air velocity while keeping a higher level of heat load. The goal of energy conservation could therefore be achieved without compromising the required level of thermal comfort.

Funding: This research received no external funding.

Conflicts of Interest: The authors declare no conflict of interest.

References

1. Schmidt, K.; Patterson, D.J. Performance results for a high efficiency tropical ceiling fan and comparisons with conventional fans Demand side management via small appliance efficiency. *Renew. Energy* **2001**, *22*, 169–176. [[CrossRef](#)]
2. Wang, X.; Song, W. FLUENT Simulation Research on Diffusion of Harmful Gases in Spray Workshop. *Energy Procedia* **2011**, *13*, 7626–7632.
3. Ho, S.H.; Rosario, L.; Rahman, M.M. Thermal comfort enhancement by using a ceiling fan. *Appl. Therm. Eng.* **2009**, *29*, 1648–1656. [[CrossRef](#)]
4. Ferro, L.M.C.; Gato, L.M.C.; Falcão, A.F.O. Design of the rotor blades of a mini hydraulic bulb-turbine. *Renew. Energy* **2011**, *36*, 2395–2403. [[CrossRef](#)]
5. Bassiouny, R.; Korah, N.S. Studying the features of air flow induced by a room ceiling-fan. *Energy Build.* **2011**, *43*, 1913–1918. [[CrossRef](#)]
6. Huang, Q.; Liu, J.; Yu, Y. Turbo air classifier guide vane improvement and inner flow field numerical simulation. *Powder Technol.* **2012**, *226*, 10–15. [[CrossRef](#)]
7. Hsiao, S.W.; Lin, H.H.; Lo, C.H. A study of thermal comfort enhancement by the optimization of airflow induced by a ceiling fan. *J. Interdiscip. Math.* **2016**, *19*, 859–891. [[CrossRef](#)]

8. Atthajariyakul, S.; Lertsatittanakorn, C. Small fan assisted air conditioner for thermal comfort and energy saving in Thailand. *Energy Convers. Manag.* **2008**, *49*, 2499–2504. [[CrossRef](#)]
9. Sonne, J.; Parker, D. Measured Ceiling Fan Performance and Usage Patterns: Implications for Efficiency and Comfort Improvement. Presented at the 1998 ACEEE Summer Study on Energy Efficiency in Buildings, Pacific Grove, CA, USA, 23–28 August 1998; Volume 11, pp. 335–341.
10. Nassif, N. Performance analysis of supply and return fans for HVAC systems under different operating strategies of economizer dampers. *Energy Build.* **2010**, *42*, 1026–1037. [[CrossRef](#)]
11. Chiang, H.C.; Pan, C.S.; Wu, H.S.; Yang, B.C. Measurement of Flow Characteristics of a Ceiling Fan with Varying Rotational Speed. In Proceedings of the Clima WellBeing Indoors, Helsinki, Finland, 10–14 June 2007.
12. Kurazumi, Y. Radiative and convective heat transfer coefficients of the human body in natural convection. *Build. Environ.* **2008**, *43*, 2142–2153. [[CrossRef](#)]
13. Sun, W.; Cheong, K.W.D.; Melikov, A.K. Subjective study of thermal acceptability of novel enhanced displacement ventilation system and implication of occupants' personal control. *Build. Environ.* **2012**, *57*, 49–57. [[CrossRef](#)]
14. Tham, K.W.; Pantelic, J. Performance evaluation of the coupling of a desktop personalized ventilation air terminal device and desk mounted fans. *Build. Environ.* **2010**, *45*, 1941–1950. [[CrossRef](#)]
15. Liu, Y.; Wang, L.; Liu, J.; Di, Y. A study of human skin and surface temperatures in stable and unstable thermal environments. *J. Therm. Biol.* **2013**, *38*, 440–448. [[CrossRef](#)]
16. Makhoul, A.; Ghali, K.; Ghaddar, N. Desk fans for the control of the convection flow around occupants using ceiling mounted personalized ventilation. *Build. Environ.* **2013**, *59*, 336–348. [[CrossRef](#)]
17. Wang, S.; Zhu, D. Application of CFD in retrofitting air-conditioning systems in industrial buildings. *Energy Build.* **2003**, *35*, 893–902. [[CrossRef](#)]
18. Jia, X.; McLaughlin, J.B.; Derksen, J.; Ahmadi, G. Simulation of a mannequin's thermal plume in a small room. *Comput. Math. Appl.* **2013**, *65*, 287–295. [[CrossRef](#)]
19. Gao, N.; Niu, J. CFD study on micro-environment around human body and personalized ventilation. *Build. Environ.* **2004**, *39*, 795–805. [[CrossRef](#)]
20. Lin, Z.; Chow, T.T.; Wang, Q.; Fong, K.F.; Chan, L.S. Validation of CFD Model for Research into Displacement Ventilation. *Archit. Sci. Rev.* **2011**, *48*, 305–316. [[CrossRef](#)]
21. Ankur, J.; Rochan, R.U.; Samarth, C.; Manish, S.; Sunil, K. Experimental investigation of the flow field of a ceiling fan. In *ASME Heat Transfer/Fluids Engineering Summer Conference*; American Society of Mechanical Engineers: New York, NY, USA, 2004; pp. 11–15.
22. Yang, Z.; Fei, J.; Song, D.; Zhao, Y.; Yu, J.; Yu, X. Effects of simulated natural air movement on thermoregulatory response during head-down bed rest. *J. Therm. Biol.* **2013**, *38*, 363–368. [[CrossRef](#)]
23. Zukowska, D.; Melikov, A.; Popiolek, Z. Impact of personal factors and furniture arrangement on the thermal plume above a sitting occupant. *Build. Environ.* **2012**, *49*, 104–116. [[CrossRef](#)]
24. Farrugia, P.S.; Micallef, A. Turbulent plumes evolving in a vertical flow under a mixed convection regime. *Int. J. Heat Mass Transf.* **2012**, *55*, 1931–1940. [[CrossRef](#)]
25. Corgnati, S.P.; Perino, M.; Fracastoro, G.V.; Nielsen, P.V. Experimental and numerical analysis of air and radiant cooling systems in offices. *Build. Environ.* **2009**, *44*, 801–806. [[CrossRef](#)]
26. Cravens, B.; Settles, G.S. A computational and experimental investigation of the human thermal plume. *J. Fluids Eng.* **2006**, *128*, 1251–1258. [[CrossRef](#)]
27. Holtedahl, P.; Joutz, F.L. Residential electricity demand in Taiwan. *Energy Econ.* **2004**, *26*, 201–224. [[CrossRef](#)]
28. Chiang, W.H.; Wang, C.Y.; Huang, J.S. Evaluation of cooling ceiling and mechanical ventilation systems on thermal comfort using CFD study in an office for subtropical region. *Build. Environ.* **2012**, *48*, 113–127.
29. Shi, Y.; Zhao, Q.; Fan, F.; Xu, G. A New Single-blade Based Hybrid CFD Method for Hovering and Forward-flight Rotor Computation. *Chin. J. Aeronaut.* **2011**, *24*, 127–135. [[CrossRef](#)]

